Generation of a bipartite mechanical cat state by performing projective Bell-state measurement on a pair of superconducting qubits

Roson Nongthombam ,* Urmimala Dewan,† and Amarendra K. Sarma ‡
Department of Physics, Indian Institute of Technology Guwahati, Guwahati-781039, India

(Received 26 April 2024; revised 31 July 2024; accepted 12 August 2024; published 26 August 2024)

Quantum state preparation and measurement of photonic and phononic Schrödinger cat states have gathered significant interest due to their implications for alternative encoding schemes in quantum computation. These schemes employ coherent state superpositions, leveraging the expanded Hilbert space provided by cavity or mechanical resonators in contrast to two-level systems. Moreover, such cat states also serve as a platform for testing fundamental quantum phenomena in macroscopic systems. In this study, we generate four bipartite phononic cat states using an entanglement swapping scheme achieved through projective Bell-state measurements on two superconducting qubits. Employing two superconducting qubits allows for the creation of bipartite phononic cat states remotely, where the two phononic resonators are separated by a far distance. Subsequently, we conduct a Bell inequality test on the bipartite cat state using the Clauser-Horne-Shimony-Holt formulation. Given that the entangled cat states are generated through entanglement swapping, our approach holds promising applications for the advancement of complex quantum network processors based on continuous-variable systems.

DOI: 10.1103/PhysRevA.110.023726

I. INTRODUCTION

Observing the quantum behavior of macroscopic mechanical structures continues to be a challenging endeavor and a significant step towards realizing quantum-acoustic state preparation and measurement. The intriguing aspect of these structures, being massive yet displaying quantum behavior, makes them important platforms for implementing various quantum technological applications and for exploring fundamental physics questions. Recent experiments have unequivocally demonstrated the quantum properties of solid-state mechanical objects [1–6]. These include interfacing mechanical objects with the strong quantum nonlinearity of superconducting qubits, leading to the field of circuit quantum acoustodynamics (cQAD) [7–13] which is analogous to the well-developed field of circuit quantum electrodynamics (cQED) [14–16]. The integration of superconducting qubits serves as a quantum-acoustic state preparation and measurement element for the mechanical system [12,13]. These state preparations and measurements are some of the basic building blocks for constructing acoustic quantum memories and processors.

A very significant quantum-acoustic state that can be prepared from the superconducting qubit-mechanical integrated system is the phononic Schrödinger cat state, defined as quantum superpositions of quasiclassical coherent states. Such phononic cat state preparation has been studied in [17,18]. Similar photonic cat states have also been studied in other various quantum systems such as circuit quantum electrodynamics [19,20], vibrational states of trapped ions [21], and propagating photon modes [22,23]. Preparing cat states has attracted wide research attention owing to its applications in implementing quantum metrology [24] and quantum information processing protocols based on continuous-variable cat states [25], as well as testing fundamental quantum phenomena in macroscopic systems [26]. One of the most fundamental tests of quantum phenomena in a quantum system is the Bell inequality test [27–30]. Bell inequality tests, performed on pairs of spatially separated entangled quantum systems, demonstrate that quantum systems do not adhere to the principle of local causality. In this work, we use the Clauser-Horne-Shimony-Holt (CHSH) [31] formulation of the Bell test to conduct the Bell inequality test on a bipartite entangled phononic cat state generated through projective Bell-state measurement on a pair of superconducting qubits [32]. The creation of bipartite photonic cat states using a single qubit is demonstrated in [20,33]. In our scheme, four bipartite phononic cat states, or four phononic Bell states, are generated on two phononic crystal mechanical resonators, interacting piezoelectrically with a pair of superconducting qubits via capacitive coupling. The two qubits are connected through a microwave cavity resonator and, through virtual excitation of the cavity photon, they become entangled, creating a qubit Bell state. Upon projective measurement of the Bell state of the qubits, each of the four bipartite phononic cat states can be distinguished. This measurement effectively swaps the entanglement from qubit-mechanical to mechanical-mechanical pairs. Such entanglement swapping schemes are pivotal in quantum repeaters, essential for realizing long-distance quantum communication and complex quantum networks [34–36]. Since the two qubits are connected via a microwave cavity bus, the phononic crystal resonator can be placed at far ends. This setup allows for the

*Contact author: n.roson@iitg.ac.in
†Contact author: d.urmimala@iitg.ac.in
‡Contact author: aksarma@iitg.ac.in

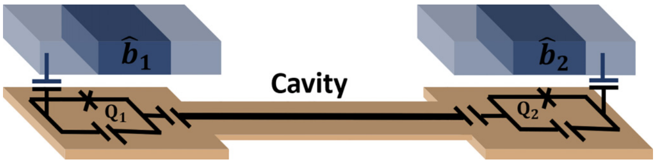

FIG. 1. Schematic of the hybrid qubit-resonator system. Two qubits denoted by Q_1 and Q_2 are capacitively coupled to the phononic crystal resonators $\hat{b}_1$ and $\hat{b}_2$, respectively [11,12]. The qubits interact piezoelectrically with the resonators. The two qubits are coupled to each other via a microwave cavity resonator. This coupling enables the interaction between the two qubits by exchanging virtual excitations of the cavity photons.

creation of bipartite phononic cat states remotely, enabling long-distance quantum state preparation. By harnessing this capability and employing entanglement swapping schemes, the bipartite phononic cat states generated in this study hold promise for practical applications in implementing quantum network processors relying on continuous-variable resonators.

We begin in Sec. II with a brief introduction of the hybrid electromechanical system under study and then discuss the generation of a resonator-qubit Bell cat state. In Sec. III, we examine the projective Bell-state measurement on the two qubits, which leads to entanglement swapping from qubit-qubit to resonator-resonator. We show how this Bell-state measurement is realized and how four bipartite phononic Bell cat states are created as a result of the projective measurement. Moving on to Sec. IV, we conduct the Bell inequality test on the bipartite cat state using the CHSH formulation.

II. QUBIT-MECHANICAL RESONATOR ENTANGLEMENT

We consider two hybrid electromechanical systems, each comprising a mechanical resonator dispersively coupled to a superconducting qubit, as shown in Fig. 1. Assuming that the two qubit-mechanical pairs are uncoupled (Appendix A), the Hamiltonian of the two hybrid systems reads

$$\hat{H}_{bq1} = \frac{\hbar}{2}\Omega_1|e_1\rangle\langle e_1| + \frac{\hbar\omega_1}{2}\hat{b}_1^\dagger\hat{b}_1 + \hbar\lambda_1\,\hat{b}_1^\dagger\hat{b}_1\,|e_1\rangle\langle e_1|, \quad (1a)$$

$$\hat{H}_{bq2} = \frac{\hbar}{2}\Omega_2|e_2\rangle\langle e_2| + \frac{\hbar\omega_2}{2}\hat{b}_2^\dagger\hat{b}_2 + \hbar\lambda_2\,\hat{b}_2^\dagger\hat{b}_2\,|e_2\rangle\langle e_2|. \quad (1b)$$

Here, Ω_1 (Ω_2) and ω_1 (ω_2) are the qubit and mechanical frequency of the first (second) hybrid system. $\hat{b}_1$ and $\hat{b}_2$ are the operators of the two mechanical resonators. In the dispersive coupling, the detuning $\delta_1 = \omega_1 - \Omega_1$ ($\delta_2 = \omega_2 - \Omega_2$) is much larger than the resonant coupling strength between the qubit and the mechanical resonator. We prepare two entangled Bell cat states by evolving the Hamiltonian $\hat{H}_{bq1}$ and $\hat{H}_{bq2}$. Initiating the qubits in the superposition state and the mechanical resonators in the coherent state, the state of the first hybrid system in the interaction frame after some time t becomes

$$|\psi\rangle_1 = (|\beta_1 e^{i\lambda_1 t}\rangle|e_1\rangle + |\beta_1\rangle|g_1\rangle)/\sqrt{2}, \quad (2)$$

where $|\beta_1\rangle$ is the coherent state of the first mechanical resonator, while $|e_1\rangle$ and $|g_1\rangle$ refer to the excited and the ground states of the first qubit, respectively. We get a similar state $|\psi\rangle_2$ for the second hybrid system. At time interval $t = (2n-1)\pi/\lambda_1$, where $n = 1, 2, 3, \ldots$, we get the Bell cat state of the qubit-mechanical system. The fidelity and entanglement of the bipartite state $|\psi\rangle_1$ in the presence of a noisy environment is shown in Fig. 2. The noisy environment is included by solving the Lindblad master equation,

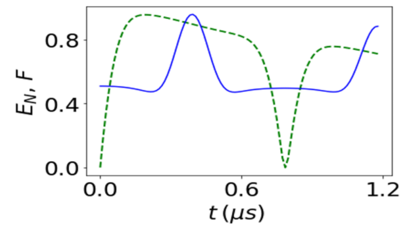

FIG. 2. Entanglement E_N (green dotted line) and fidelity F (solid blue line) measurement of the state $|\psi\rangle_1$ in the presence of thermal noise. As expected, the state $|\psi\rangle_1$ evolves into the Bell cat state $|\psi\rangle_1 = (-\beta_1\rangle|e_1\rangle + |\beta_1\rangle|g_1\rangle)/\sqrt{2}$ at the interval π/λ_1, $3\pi/\lambda_1$,..., and so on. The parameters used are $\beta_1 = \sqrt{2}$, $\gamma_1 = 0.1$ MHz, $\Gamma_1 = 0.1$ MHz, $n_{th} = 0.03$, and $\lambda_1 = 8$ MHz.

$$\dot{\hat{\rho}}_1 = -\frac{i}{\hbar}[\hat{H}_{\text{int}}, \hat{\rho}_1] + \gamma_1(n_1+1)\mathcal{L}[\hat{b}_1] + \gamma_1 n_1\mathcal{L}[\hat{b}_1^\dagger] + \Gamma_1\mathcal{L}[\hat{\sigma}_-] + \Gamma_1\mathcal{L}[\hat{\sigma}_+] + \Gamma_1\mathcal{L}[\hat{\sigma}_z], \quad (3)$$

where $\mathcal{L}[\hat{o}] = (2\hat{o}\hat{\rho}\hat{o}^\dagger - \hat{o}^\dagger\hat{o}\hat{\rho} - \hat{\rho}\,\hat{o}^\dagger\,\hat{o})/2$ with $\hat{o} \in \{\hat{b}_1, \hat{\sigma}_-, \hat{\sigma}_z\}$. γ_1 and Γ_1 are the decay rates of the mechanical resonator and the qubit, respectively. The entanglement of the qubit-mechanical bipartite system is computed using the relation $E_N(\hat{\rho}_1) = \log_2||\hat{\rho}_1^{T_A}||$, where $\hat{\rho}_1^{T_A}$ is the trace norm of the partial transpose of the bipartite mixed state $\hat{\rho}_1$ [37,38]. As shown in the figure, the fidelity (F) reaches near one at the interval $t = 0.39$ μs, 1.18 μs, and so on, for coupling constant $\lambda_1 = 8$ MHz. Therefore, the qubit-mechanical bipartite system evolves into a Bell cat state at the interval of π.

III. GENERATION OF BIPARTITE CAT STATE

After the interaction time of $t_1 = \pi/\lambda_1$ ($t_2 = \pi/\lambda_2$), the state of the qubit-mechanical bipartite state [Eq. (2)] becomes $|\psi\rangle_1 = (| - \beta_1\rangle|e_1\rangle + |\beta_1\rangle|g_1\rangle)/\sqrt{2}$ ($|\psi\rangle_2 = (| - \beta_2\rangle|e_2\rangle + |\beta_2\rangle|g_2\rangle)/\sqrt{2}$). The state of the combined system, $|\Psi\rangle$, is then given by the tensor product of the states of the two hybrid systems, i.e., $|\Psi\rangle = |\psi\rangle_1|\psi\rangle_2$,

$$|\Psi\rangle = \tfrac{1}{2}[|e_1 e_2 - \beta_1 - \beta_2\rangle + |e_1 g_2 - \beta_1 + \beta_2\rangle + |g_1\, e_2\, \beta_1 - \beta_2\rangle + |g_1\, g_2\, \beta_1\, \beta_2\rangle], \quad (4)$$

where $|\beta_2\rangle$ is the coherent amplitude of the second resonator. In terms of the Bell's basis, $|\phi^{\pm}\rangle = (1/\sqrt{2})(|e_1 e_2\rangle \pm i|g_1 g_2\rangle$ and $|\psi^{\pm}\rangle = (1/\sqrt{2})(|e_1 g_2\rangle \pm i|g_1 e_2\rangle$, the wave function of the combined system [Eq. (4)] can be rearranged to

$$\begin{aligned}|\Psi\rangle = \frac{1}{2\sqrt{2}}[&|\phi^+\rangle(| - \beta_1 - \beta_2\rangle - i|\beta_1\,\beta_2\rangle) \\ &+ |\phi^-\rangle(| - \beta_1 - \beta_2\rangle + i|\beta_1\,\beta_2\rangle) \\ &+ |\psi^+\rangle(| - \beta_1\,\beta_2\rangle - i|\beta_1 - \beta_2\rangle) \\ &+ |\psi^-\rangle(| - \beta_1\,\beta_2\rangle + i|\beta_1 - \beta_2\rangle)].\end{aligned} \quad (5)$$

Therefore, by measurement of the Bell's states $|\phi^{\pm}\rangle$ and $|\psi^{\pm}\rangle$, the two mechanical resonators are projected into the bipartite cat states $|C'_{\mp}\rangle = \mathcal{N}'_{\mp}(|-\beta_1 - \beta_2\rangle \mp i|\beta_1\,\beta_2\rangle)$ and $|C_{\mp}\rangle = \mathcal{N}_{\mp}(|-\beta_1\,\beta_2\rangle \mp i|\beta_1 - \beta_2\rangle)$, respectively. The Bell-state measurement of the two qubits is performed by first switching on the interaction between them $[\hbar J'(\hat{\sigma}_1^-\hat{\sigma}_2^+ + \hat{\sigma}_1^+\hat{\sigma}_2^-)$; refer to Appendix A]. This interaction, which will entangle the two qubits, is achieved by red detuning the second qubit from the cavity and blue detuning the same qubit from the second resonator. Such detuning arrangement or dispersive coupling allows the exchange of virtual cavity photons with the qubits. Since the actual cavity photon is not excited, the qubit-qubit interaction generated in this way is less sensitive to the quality factor of the cavity and hence can easily achieve maximally entangled states. If we consider resonant cavity-qubit coupling, then the maximally entangled state of the qubit-qubit interaction will be further deteriorated by cavity decay. The virtual interaction between the two qubits only produces two of the four Bell states, $|\psi^{\pm}\rangle$. Instead of transforming from one Bell state to the other for every measurement, we generate all four of the Bell states simultaneously. To generate all four Bell states, we continuously drive the two qubits, resulting in two dressed states, $|\pm\rangle_j = [1/\sqrt(2)](|g\rangle_j \pm e^{i\Phi_j}|e\rangle_j)$, $j = 1, 2$. The qubit cannot go into transitions between different dressed states under the conditions $\Phi_1 = \Phi_2 = \Phi$ and $|A_1 - A_2| \gg |J'|$, where A_j and Φ_j are the drive amplitude and phase. When the phases of both the driving fields are reversed right in the middle of the two-qubit interaction time, then the dressed state of the two qubits evolves to $|++\rangle_\tau = (1/2)(i|\phi^-\rangle + |\phi^+\rangle + i|\psi^-\rangle + |\psi^+\rangle)$, where $\tau = \pi/(2J')$. The above protocol for producing the dressed state $|++\rangle_\tau$ is known as the dressed-state phase gate. In Figs. 3(a) and 3(b), we plot the fidelity of the dressed state generated through the dressed-state phase gate. The measurement fidelity of the Bell state is dependent on the fidelity of the dressed-state phase gate. The four Bell states generated through the dressed-state phase gate can be mapped onto the computational basis as $|\phi^+\rangle \to (0_1 0_2)$, $|\phi^-\rangle \to (1_1 1_2)$, $|\psi^+\rangle \to (1_1 0_2)$, and $|\psi^-\rangle \to (0_1 1_2)$ [32,39] (see Appendix B). Therefore, based on the measurement outcomes of the two qubits in the computational basis, all four bipartite cat states of the resonators are generated. The sequence of operations performed in our scheme to generate the bipartite cat state is illustrated in Fig. 3(c).

The above protocol is realized in the noisy environment by first independently evolving the two qubit-mechanical hybrid systems under the Lindblad master equation and then performing the projective measurement on the density matrix of the combined system, $\hat{\rho} = \hat{\rho}_1\hat{\rho}_2$. The reduced density matrices of the four bipartite Bell cat states after the projective Bell-state measurement on the two qubits read

$$\hat{\rho}_{C'_{\mp}} = \frac{\langle\phi^{\pm}|\hat{\rho}|\phi^{\pm}\rangle}{\mathrm{tr}(\langle\phi^{\pm}|\hat{\rho}|\phi^{\pm}\rangle)}, \quad \hat{\rho}_{C_{\mp}} = \frac{\langle\psi^{\pm}|\hat{\rho}|\psi^{\pm}\rangle}{\mathrm{tr}(\langle\psi^{\pm}|\hat{\rho}|\psi^{\pm}\rangle)}. \tag{6}$$

Constructing the reduced density matrix [Eq. (6)] on the number basis will require a huge subspace, and performing joint state tomography on the resonators will be experimentally challenging. So, we reconstruct the density matrix into a two-level system subspace by projecting into the basis state

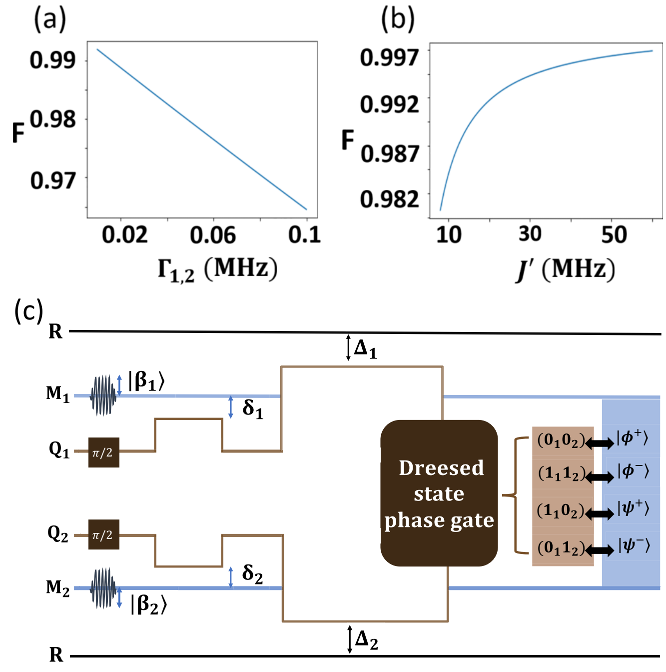

FIG. 3. The change in fidelity of the dressed state $|++\rangle_\tau$ with respect to (a) decay rate $\Gamma_{1,2}$ and (b) coupling strength J'. The coupling strength in (a) is $J' = 8$ MHz and the decay rates in (b) are $\Gamma_{1,2} = 0.1$ MHz. (c) Sequence of qubit detuning and Bell-state preparation and measurement. Both the qubits Q_1 and Q_2 are initially prepared in the superposition state by applying a $\pi/2$ pulse. Similarly, mechanical resonators (M_1 and M_2) are initially prepared in coherent states ($|\beta_1\rangle$ and $|\beta_2\rangle$) by driving it on resonance with a microwave drive. We then initiate the qubit-mechanical dispersive interaction by detuning the qubits to δ_1 and δ_2 with respect to the resonators. After time $t_1 = t_2 = \pi/\lambda_{1,2}$, we bring the qubits back to their idle frequencies, terminating the qubit-mechanical dispersive interaction. Now we switch on the qubit-qubit interaction by detuning the qubits to Δ_1 and Δ_2 with respect to the microwave resonator R. After time $\tau = \pi/2J'$, we bring the qubits back to their idle frequencies and start the Bell-state measurements. During the time τ, the qubits are continuously driven, generating the dressed-state phase gate.

$(|\beta_{1,2}\rangle, |-\beta_{1,2}\rangle)$. The Pauli operators for the resonator can be obtained by measuring the displaced phonon number parity observable $\hat{P}_{\beta_1} = \hat{D}_{\beta_1}\hat{P}\hat{D}^{\dagger}_{\beta_1}$, where $\hat{D}_{\beta_1}$ is the displacement operator and $\hat{P}$ is the phonon number parity operator [13,26]. The Pauli operators for the resonator mode become

$$\hat{X}_{\beta_1} = \hat{P}_0, \quad \hat{I}_{\beta_1} = [\hat{P}_{\beta_1} + \hat{P}_{-\beta_1}],$$
$$\hat{Y}_{\beta_1} = \hat{P}_{\frac{-i\pi}{8\beta_1^*}}, \quad \hat{Z}_{\beta_1} = [\hat{P}_{\beta_1} - \hat{P}_{-\beta_1}]. \tag{7}$$

We have assumed a large orthonormal cat state, i.e., $\langle\beta_1|-\beta_1\rangle \ll 1$. Four Wigner functions $[W(\alpha) = \frac{2}{\pi}\langle P_\alpha\rangle$, where $\alpha = 0, \beta, -\beta, -i\pi/8\beta^*]$ are required to reconstruct the state. The basis for the Pauli operators is $(|\beta_1\rangle, |-\beta_1\rangle)$ which is analogous to the qubit basis $(|e\rangle, |g\rangle)$. Similar Pauli operators and basis $(|\beta_2\rangle, |-\beta_2\rangle)$ can be generated for the second resonator using the same approach. In Fig. 4, we plot the joint density matrix of the two resonators in the joint basis states $(|\beta_1\,\beta_2\rangle$, $|-\beta_1\,\beta_2\rangle$, $|\beta_1\,-\beta_2\rangle$, and $|-\beta_1\,-\beta_2\rangle)$. We observe four

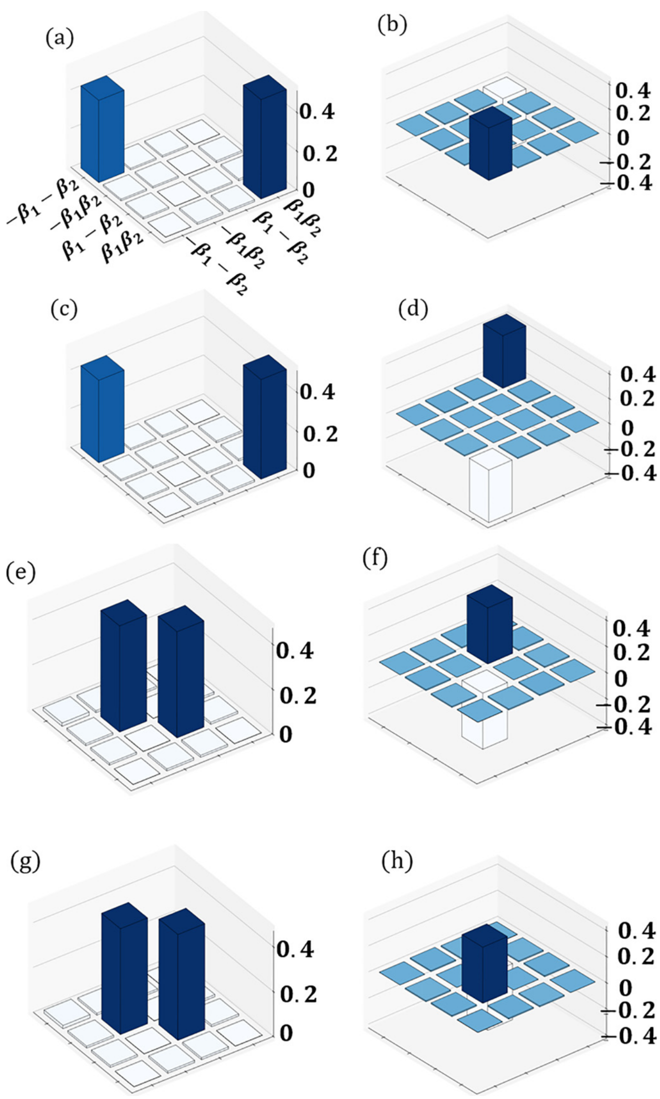

FIG. 4. Construction of the four bipartite phononic cat state density matrices in the two-level subspace. (a) and (b) [(c) and (d)] represent the real and imaginary parts of $\hat{\rho}_{C'_-}$ ($\hat{\rho}_{C'_+}$), respectively. Similarly, (e) and (f) [(g) and (h)] represent the real and imaginary parts of $\hat{\rho}_{C_-}$ ($\hat{\rho}_{C_+}$), respectively. The density matrices resemble those of the two-qubit Bell state [32]. We have used the resonator coherent amplitudes $\beta_{1,2} = \sqrt{2}$.

bipartite cat states having fidelities $F_{C'_-} = 0.919$, $F_{C'_+} = 0.919$, $F_{C_-} = 0.92$, and $F_{C_+} = 0.92$ and entanglements $E_{C'_-} = 0.799$, $E_{C'_+} = 0.799$, $E_{C_-} = 0.799$, and $E_{C_+} = 0.799$. The dip in the density matrix element is mainly attributed to the relaxation and decoherence effect of the two qubits, as well as the relaxation of the two resonators. As shown in Fig. 5, the fidelity of the bipartite cat state can be significantly improved by improving the decay rates of both the qubit and the phononic resonator. For example, we get $F_{C'_-} = 0.9581$, $F_{C'_+} = 0.9581$, $F_{C_-} = 0.9581$, and $F_{C_+} = 0.9581$ and entanglements $E_{C'_-} = 0.895$, $E_{C'_+} = 0.895$, $E_{C_-} = 0.895$, and $E_{C_+} = 0.895$ for decay rates $\gamma_{1,2} = 0.05$ MHz and $\Gamma_{1,2} = 0.05$ MHz. In Fig. 5, we have generated the fidelity variation for the $|C_+\rangle$ state. We get similar plots for the other cat states too. In addition to the decays resulting from direct contact with the noisy environment,

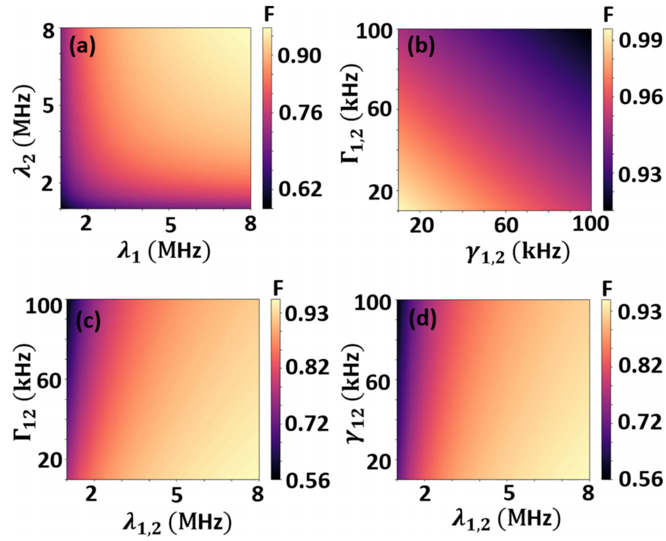

FIG. 5. Fidelity of the bipartite cat state $|C_+\rangle$ as a function of (a) λ_1 and λ_2, (b) γ_1 and Γ_1, (c) Γ_1 and λ_1, and (d) λ_1 and γ_1. The decay rates in (a) are $\gamma_{1,2} = 0.1$ MHz and $\Gamma_{1,2} = 0.1$ MHz. The coupling strengths in (b) are $\lambda_{1,2} = 8$ MHz. In (c), the decay rates of the first and second resonators are $\gamma_{1,2} = 0.1$ MHz. The qubits decay rates in (d) are $\Gamma_{1,2} = 0.1$ MHz. In all four plots, the variable parameters are simultaneously varied for both of the qubit-mechanical systems. As expected, we observe an increase in fidelity when the decay rates decrease and coupling constant increases.

the other factors that lead to the infidelities of the prepared state include readout errors while measuring the mechanical resonators and errors while performing the Bell measurement. The four bipartite cat states resemble the traditional qubit Bell states generated using a HADAMARD and CNOT gate in a quantum circuit. Going by this similarity, the scheme proposed here could be used to implement an entanglement gate for a continuous-variable resonator qubit and may find applications in the bosonic-based quantum processors.

IV. BELL'S TEST OF THE RESONATOR BIPARTITE CAT STATE

The bipartite entangled cat states of the two resonators generated on a conditional Bell-state measurement of the two qubits can be used as a platform to test the Bell's inequality in a macroscopic quantum system. Here, we perform this test by calculating the expectation values of all the correlations of the measurement outcomes measured locally at the two resonators and then determine the Clauser-Horne-Shimony-Holt (CHSH) value $S = \langle X_1X_2\rangle + \langle X_1Y_2\rangle - \langle Y_1X_2\rangle + \langle Y_1Y_2\rangle$, where, X_1 (X_2) and Y_1 (Y_2) are the observables of the first (second) resonator. The observables are measured in the resonator-qubit subspace discussed above. As per CHSH inequality, a system is said to be classically correlated if $|S| \leqslant 2$ and quantumly if $2 < |S| \leqslant 2\sqrt{2}$. The correlation of the observables is measured by first choosing two arbitrary values of β'_1 and β'_2 corresponding to X_1, Y_1 and X_2, Y_2, respectively. We then rotate the resonator detector basis by coherently displacing the observables X_1 and Y_1 to $X_\alpha = D_{-i\alpha}X_1D_{i\alpha}$ and $Y_\alpha = D_{-i\alpha}Y_1D_{i\alpha}$, or

$$X_\alpha = X_1\ \cos 2(\alpha\beta_1'^* + \alpha^*\beta_1') + Y_1 \sin 2(\alpha\beta_1'^* + \alpha^*\beta_1'),$$
$$Y_\alpha = Y_1\ \cos 2(\alpha\beta_1'^* + \alpha^*\beta_1') - X_1 \sin 2(\alpha\beta_1'^* + \alpha^*\beta_1'). \quad (8)$$

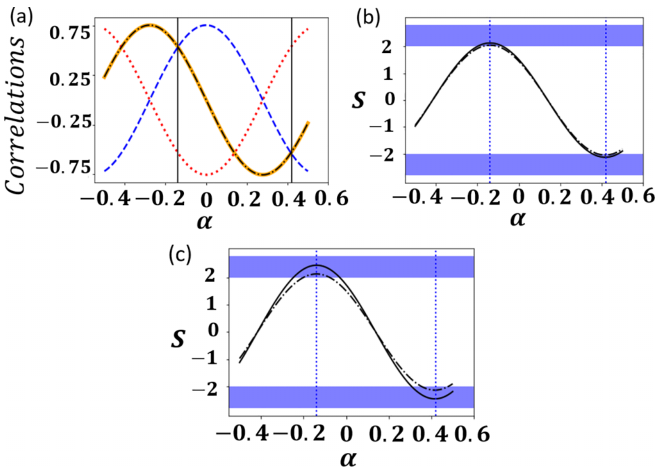

FIG. 6. Measurement correlations and inequality test are conducted with respect to the change in the displacement amplitude α for mechanical coherence strength $\beta_{1,2} = \sqrt{2}$. (a) The expectation values of all the joint measurement correlations between the two resonators. The red dotted, blue dashed, black dash-dotted, and solid orange lines represent the measurement correlations $\langle Y_\alpha X_2\rangle$, $\langle X_\alpha Y_2\rangle$, $\langle Y_\alpha Y_2\rangle$, and $\langle X_\alpha X_2\rangle$, respectively. (b) The CHSH value S of the Bell inequality. The solid and dash-dotted lines correspond to the coupling strengths $\lambda_1 = \lambda_2 = 8$ MHz and $\lambda_1 = \lambda_2 = 7$ MHz, respectively. For both cases, the maximum $|S|$ values occur at $\alpha_1 = -0.14$ and $\alpha_2 = 0.41$, denoted by the two dotted vertical lines, with corresponding values of 2.132 and 2.049. The decay rates in (b) are $\gamma_{1,2} = 0.1$ MHz and $\Gamma_{1,2} = 0.1$ MHz. For different decay rates $\gamma_{1,2} = 0.05$ MHz and $\Gamma_{1,2} = 0.05$ MHz, we get $|S| = 2.454$ for $\lambda_1 = \lambda_2 = 8$ MHz, as shown in (c) (solid line). The dash-dotted line in (c) is for $\gamma_{1,2} = 0.1$ MHz, $\Gamma_{1,2} = 0.1$ MHz, and $\lambda_1 = \lambda_2 = 8$ MHz, which is similar to the solid line in (b). The shaded horizontal lines represent the regions of the quantum limit.

Here, α is the coherent displacement amplitude of the resonator. By changing the amplitude α, we are able to rotate the measurement basis direction and perform measurements at all possible orientations of the detectors. The $|S|$ value for the state $|C_+\rangle$ is shown in Fig. 6(b). We observe a maximum $|S|$ value when $\beta'_{1,2} = \beta_{1,2}$ and at the displacement amplitude $\alpha_1 = -0.14$ and $\alpha_2 = 0.41$. Furthermore, the α_1, α_2, and β'_1 amplitudes corresponding to the maximum $|S|$ value satisfy the relations $4\alpha_2\beta'_1 = 3\pi/4$ and $4\alpha_1\beta'_1 = -\pi/4$. The corresponding observables [Eq. (8)] at these amplitudes become $X_{\alpha_1} = (X_1 - Y_1)/\sqrt{2}$ and $Y_{\alpha_1} = (X_1 + Y_1)/\sqrt{2}$. Therefore, the $|S|$ value observed in the figure exceeds the classical bound limit and attains a value which is less than the ideal quantum bound limit $2\sqrt{2}$ [see Figs. 6(b) and 6(c)]. As we decrease the decay rates of the resonators and the qubits, the maximum attainable $|S|$ value also increases, as shown in Fig. 6(c). The expectation values of all the measurement correlations are also shown in Fig. 6(a). The behavior of these correlations as we change the displacement amplitude α resembles the one observed in two-qubit Bell test experiments [30]. By integrating two phononic crystal resonators into the experimental arrangement typically employed for conducting a loophole-free Bell test with two superconducting qubits [30], our proposed approach could be employed to examine the Bell inequality of a phononic cat state. Additionally, the bipartite phononic cat state generated through entanglement swapping in this work could hold significant practical implications for the advancement of complex quantum network processors based on continuous-variable resonators.

V. CONCLUSION

In conclusion, we propose a scheme to generate four bipartite phononic cat states by performing a projective Bell-state measurement on two superconducting qubits. Initially uncoupled phononic crystal resonators, each coupled to a different superconducting qubit, become entangled through entanglement swapping from qubit-mechanical to mechanical-mechanical interactions. Displaced phonon parity measurement is done to generate a joint density matrix of the two resonators in two-level subspace. These joint density matrices resemble those of traditional qubit Bell states generated using a HADAMARD and CNOT gate in a quantum circuit. Subsequently, we investigate the Bell inequality test using the CHSH formulation. The expectation values of the measurement correlations and the S values of the CHSH inequality test obtained here are akin to those observed in [30] for two superconducting qubits. The bipartite phononic cat state generated through entanglement swapping in this work may be useful in implementing quantum network processors based on continuous-variable resonators. Furthermore, the scheme presented in this work also serves as a platform for studying the Bell inequality test in a continuous-variable system.

ACKNOWLEDGMENTS

R.N. gratefully acknowledges the support of a research fellowship from CSIR, Government of India. U.D. gratefully acknowledges a research fellowship from MoE, Government of India. A.K.S. and R.N. acknowledges the grant from MoE, Government of India (Grant No. MoE-STARS/STARS-2/2023-0161).

APPENDIX A: DISPERSIVE HAMILTONIAN

The interaction part of the complete Hamiltonian, including the cavity resonator connecting the two qubits, is given by the Jaynes-Cummings interaction,

$$\hat{H}_{\text{int}} = g_1(\hat{b}_1^\dagger\hat{\sigma}_-^1 + \hat{b}_1\hat{\sigma}_+^1) + g_2(\hat{b}_2^\dagger\hat{\sigma}_-^2 + \hat{b}_2\hat{\sigma}_+^2) + G_1(\hat{a}^\dagger\hat{\sigma}_-^1 + \hat{a}\hat{\sigma}_+^1) + G_2(\hat{a}^\dagger\hat{\sigma}_-^2 + \hat{a}\hat{\sigma}_+^2). \tag{A1}$$

Here, g_1 (g_2) and G_1 (G_2) are the resonant coupling strength of mechanical-qubit and qubit-cavity interactions, respectively. $\hat{a}$ and $\hat{a}^\dagger$ are the creation and annihilation operators of the cavity resonator. We blue detune the first resonator from the first qubit ($\delta_1 = \omega_1 - \Omega_1$), second qubit from the cavity resonator ($\Delta_2 = \omega - \Omega_2$), and red detune the cavity from the first qubit ($\Delta_1 = \Omega_1 - \omega$), second resonator from the second qubit ($\delta_2 = \Omega_2 - \omega_2$). Here, ω refers to the cavity resonance frequency. Because of the detuning, we can transform the Jaynes-Cummings interaction [Eq. (A1)] into a dispersive one by performing a unitary operation,

$U = \exp\{ g_1/\delta_1 (\hat{b}_1^\dagger \hat{\sigma}_-^1 - \hat{b}_1 \hat{\sigma}_+^1) + g_2/\delta_2(\hat{b}_2\hat{\sigma}_+^2 - \hat{b}_2^\dagger \hat{\sigma}_-^2) + G_1/\Delta_1(\hat{a}\hat{\sigma}_+^1 - \hat{a}^\dagger\hat{\sigma}_-^1) + G_2/\Delta_2(\hat{a}^\dagger\hat{\sigma}_-^2 - \hat{a}\hat{\sigma}_+^2)\}$ on $\hat{H}_{\text{int}}$,

$$\begin{aligned}\hat{H}_{\text{dis}} = \hbar\big(\eta_1\hat{\sigma}_z^1 + \eta_2\hat{\sigma}_z^2\big)\hat{a}^\dagger\hat{a} + \hbar\lambda_1\hat{\sigma}_z^1\hat{b}_1^\dagger\hat{b}_1 + \hbar\lambda_2\hat{\sigma}_z^2\hat{b}_2^\dagger\hat{b}_2 \\ + \hbar J(\hat{\sigma}_1^-\hat{\sigma}_2^+ + \hat{\sigma}_1^+\hat{\sigma}_2^-) + \hbar\chi_1(\hat{a}\hat{b}_1^\dagger + \hat{b}_1\hat{a}^\dagger)\hat{\sigma}_1^z \\ + \hbar\chi_2(\hat{a}\hat{b}_2^\dagger + \hat{b}_2\hat{a}^\dagger)\hat{\sigma}_2^z,\end{aligned} \tag{A2}$$

where $\eta_1 = G_1^2/\Delta_1$, $\eta_2 = G_2^2/\Delta_2$, $\lambda_1 = g_1^2/\delta_1$, $\lambda_2 = g_2^2/\delta_2$, $J = G_1G_2(1/\Delta_1 - 1/\Delta_2)$, $\chi_1 = g_1G_1(1/\delta_1 - 1/\Delta_1)$, and $\chi_2 = g_2G_2(1/\Delta_2 - 1/\delta_2)$. The first term in the Hamiltonian (A2) can be neglected since the cavity remains in the ground state. We can ignore the last three terms if we only dispersively detune the qubit-mechanical pair and the detuned qubit frequency is way off from the cavity frequency such that there is no interaction between the qubit and the cavity [32]. If the qubit-mechanical and qubit-cavity detuning are simultaneous, then by choosing $\Delta_1 = \Delta_2$, $\delta_1 = \Delta_1$, and $\delta_2 = \Delta_2$, we can also neglect the last terms [12,40]. The remaining two interacting terms are the ones used in Hamiltonian (1a) and (1b). Thus, we see that by changing the detuning, we can independently evolve the two qubit-resonator pairs. In our scheme, we first evolve the qubit-mechanical pair dispersively up to a certain time period. We then bring back the qubits to their idle frequencies so that the interaction between the qubit and mechanical resonator is turned off [13]. We now initiate the qubit-qubit interaction (fourth term) by detuning back the qubit with respect to the cavity in order to perform the Bell-state measurement. This can be done in two ways: First, by choosing $\Delta_1 \neq \Delta_2$, or second, by red detuning the second qubit from the cavity and blue detuning the second qubit from the second resonator. In the second approach, the coupling constant J becomes $J' = G_1G_2(1/\Delta_1 + 1/\Delta_2')$, where $\Delta_2' = \Omega_2 - \omega$. The coupling sequence is shown in Fig. 3(d).

APPENDIX B: BELL STATE OF THE TWO QUBITS

In order to distinguish all the Bell states of the two qubits, we resonantly drive the qubits individually. In the interaction frame, the Hamiltonian of the two-qubit interaction is

$$\hat{H} = \hbar\left(J'\hat{\sigma}_1^+\hat{\sigma}_2^- + \sum_{j=1,2} A_j e^{-i\Phi_j}\sigma_j^+\right) + \text{H.c.} \tag{B1}$$

Here, A_j and Φ_j are the Rabi frequency and phase, respectively, of the drive applied to the qubits. We have assumed that $J' \gg \lambda_1, \lambda_2$. The drive produces two dressed states, $|\pm\rangle_j = [1/\sqrt(2)](|g_j\rangle \pm e^{i\Phi_j}|e\rangle_j)$. The qubit cannot go into transitions between different dressed states under the conditions $\Phi_1 = \Phi_2 = \Phi$ and $|A_1 - A_2| \gg |J'|$. Then the Hamiltonian (B1) in the dressed-state basis reduces to [32,39]

$$\hat{H}_{\text{eff}} = \frac{1}{2}\hbar J' S_{z1}S_{z2} + \hbar \sum_{j=1,2} A_j S_{zj}. \tag{B2}$$

Here, $S_zj = |+\rangle_j\langle+|_j - |-\rangle_j\langle-|_j$. If the phases of both driving fields are reversed right in the middle of the two-qubit interaction time, then the dressed state $|+\rangle_1|+\rangle_2$ evolves to $|++\rangle_t = \exp(iJ't/2)|+\rangle_1|+\rangle_2$. At time $\tau = \pi/2J'$, the dressed state becomes $|++\rangle_\tau = (1/2)(i|\phi^-\rangle + |\phi^+\rangle + i|\psi^-\rangle + |\psi^+\rangle)$. In the computational basis ($|0\rangle$, $|1\rangle$), the state $|++\rangle_\tau$ can be obtained by applying the unitary operator,

$$U = \begin{bmatrix} 1 & 0 & 0 & i \\ 0 & 1 & i & 0 \\ 0 & i & 1 & 0 \\ i & 0 & 0 & 1 \end{bmatrix}. \tag{B3}$$

Therefore, in the computational basis, the Bell state $|\phi^+\rangle$ is mapped to $|0_10_2\rangle$, i.e., $U|0_10_2\rangle = |\phi^+\rangle$. Similarly, $|\phi^-\rangle$, $|\psi^+\rangle$, and $|\psi^-\rangle$ are mapped onto $|1_11_2\rangle$, $|1_10_2\rangle$, $|0_11_2\rangle$.

[1] A. D. O'Connell, M. Hofheinz, M. Ansmann, R. C. Bialczak, M. Lenander, E. Lucero, M. Neeley, D. Sank, H. Wang, M. Weides *et al.*, Nature (London) **464**, 697 (2010).

[2] P. Arrangoiz-Arriola, E. A. Wollack, Z. Wang, M. Pechal, W. Jiang, T. P. McKenna, J. D. Witmer, R. Van Laer, and A. H. Safavi-Naeini, Nature (London) **571**, 537 (2019).

[3] Y. Chu, P. Kharel, T. Yoon, L. Frunzio, P. T. Rakich, and R. J. Schoelkopf, Nature (London) **563**, 666 (2018).

[4] S. Kotler, G. A. Peterson, E. Shojaee, F. Lecocq, K. Cicak, A. Kwiatkowski, S. Geller, S. Glancy, E. Knill, R. W. Simmonds *et al.*, Science **372**, 622 (2021).

[5] C. Ockeloen-Korppi, E. Damskägg, J.-M. Pirkkalainen, M. Asjad, A. Clerk, F. Massel, M. Woolley, and M. Sillanpää, Nature (London) **556**, 478 (2018).

[6] G. S. MacCabe, H. Ren, J. Luo, J. D. Cohen, H. Zhou, A. Sipahigil, M. Mirhosseini, and O. Painter, Science **370**, 840 (2020).

[7] J.-M. Pirkkalainen, S. Cho, J. Li, G. Paraoanu, P. Hakonen, and M. Sillanpää, Nature (London) **494**, 211 (2013).

[8] F. Lecocq, J. D. Teufel, J. Aumentado, and R. W. Simmonds, Nat. Phys. **11**, 635 (2015).

[9] A. Bienfait, K. J. Satzinger, Y. Zhong, H.-S. Chang, M.-H. Chou, C. R. Conner, É. Dumur, J. Grebel, G. A. Peairs, R. G. Povey, and A. N. Cleland, Science **364**, 368 (2019).

[10] M. LaHaye, J. Suh, P. Echternach, K. C. Schwab, and M. L. Roukes, Nature (London) **459**, 960 (2009).

[11] N. R. A. Lee, Y. Guo, A. Y. Cleland, E. A. Wollack, R. G. Gruenke, T. Makihara, Z. Wang, T. Rajabzadeh, W. Jiang, F. M. Mayor, P. Arrangoiz-Arriola, C. J. Sarabalis, and A. H. Safavi-Naeini, PRX Quantum **4**, 040342 (2023).

[12] E. A. Wollack, A. Y. Cleland, R. G. Gruenke, Z. Wang, P. Arrangoiz-Arriola, and A. H. Safavi-Naeini, Nature (London) **604**, 463 (2022).

[13] U. von Lüpke, Y. Yang, M. Bild, L. Michaud, M. Fadel, and Y. Chu, Nat. Phys. **18**, 794 (2022).

[14] A. Blais, A. L. Grimsmo, S. M. Girvin, and A. Wallraff, Rev. Mod. Phys. **93**, 025005 (2021).

[15] A. Wallraff, D. I. Schuster, A. Blais, L. Frunzio, R.-S. Huang, J. Majer, S. Kumar, S. M. Girvin, and R. J. Schoelkopf, Nature (London) **431**, 162 (2004).

[16] A. Blais, J. Gambetta, A. Wallraff, D. I. Schuster, S. M. Girvin, M. H. Devoret, and R. J. Schoelkopf, Phys. Rev. A **75**, 032329 (2007).
[17] D. Radić, S.-J. Choi, H. C. Park, J. Suh, R. I. Shekhter, and L. Y. Gorelik, npj Quantum Inf. **8**, 74 (2022).
[18] M. Bild, M. Fadel, Y. Yang, U. Von Lüpke, P. Martin, A. Bruno, and Y. Chu, Science **380**, 274 (2023).
[19] B. Vlastakis, G. Kirchmair, Z. Leghtas, S. E. Nigg, L. Frunzio, S. M. Girvin, M. Mirrahimi, M. H. Devoret, and R. J. Schoelkopf, Science **342**, 607 (2013).
[20] C. Wang, Y. Y. Gao, P. Reinhold, R. W. Heeres, N. Ofek, K. Chou, C. Axline, M. Reagor, J. Blumoff, K. Sliwa *et al.*, Science **352**, 1087 (2016).
[21] D. J. Wineland, Rev. Mod. Phys. **85**, 1103 (2013).
[22] B. Hacker, S. Welte, S. Daiss, A. Shaukat, S. Ritter, L. Li, and G. Rempe, Nat. Photon. **13**, 110 (2019).
[23] A. Ourjoumtsev, R. Tualle-Brouri, J. Laurat, and P. Grangier, Science **312**, 83 (2006).
[24] M. Tatsuta, Y. Matsuzaki, and A. Shimizu, Phys. Rev. A **100**, 032318 (2019).
[25] J. Guillaud and M. Mirrahimi, Phys. Rev. X **9**, 041053 (2019).
[26] B. Vlastakis, A. Petrenko, N. Ofek, L. Sun, Z. Leghtas, K. Sliwa, Y. Liu, M. Hatridge, J. Blumoff, L. Frunzio *et al.*, Nat. Commun. **6**, 8970 (2015).
[27] B. Hensen, H. Bernien, A. E. Dréau, A. Reiserer, N. Kalb, M. S. Blok, J. Ruitenberg, R. F. Vermeulen, R. N. Schouten, C. Abellán *et al.*, Nature (London) **526**, 682 (2015).
[28] M. Giustina, M. A. M. Versteegh, S. Wengerowsky, J. Handsteiner, A. Hochrainer, K. Phelan, F. Steinlechner, J. Kofler, J.-A. Larsson, C. Abellán, W. Amaya, V. Pruneri, M. W. Mitchell, J. Beyer, T. Gerrits, A. E. Lita, L. K. Shalm, S. W. Nam, T. Scheidl, R. Ursin *et al.*, Phys. Rev. Lett. **115**, 250401 (2015).
[29] L. K. Shalm, E. Meyer-Scott, B. G. Christensen, P. Bierhorst, M. A. Wayne, M. J. Stevens, T. Gerrits, S. Glancy, D. R. Hamel, M. S. Allman, K. J. Coakley, S. D. Dyer, C. Hodge, A. E. Lita, V. B. Verma, C. Lambrocco, E. Tortorici, A. L. Migdall, Y. Zhang, D. R. Kumor *et al.*, Phys. Rev. Lett. **115**, 250402 (2015).
[30] S. Storz, J. Schär, A. Kulikov, P. Magnard, P. Kurpiers, J. Lütolf, T. Walter, A. Copetudo, K. Reuer, A. Akin *et al.*, Nature (London) **617**, 265 (2023).
[31] J. F. Clauser, M. A. Horne, A. Shimony, and R. A. Holt, Phys. Rev. Lett. **23**, 880 (1969).
[32] W. Ning, X.-J. Huang, P.-R. Han, H. Li, H. Deng, Z.-B. Yang, Z.-R. Zhong, Y. Xia, K. Xu, D. Zheng, and S.-B. Zheng, Phys. Rev. Lett. **123**, 060502 (2019).
[33] Z. Wang, Z. Bao, Y. Wu, Y. Li, W. Cai, W. Wang, Y. Ma, T. Cai, X. Han, J. Wang *et al.*, Sci. Adv. **8**, eabn1778 (2022).
[34] N. Sangouard, C. Simon, N. Gisin, J. Laurat, R. Tualle-Brouri, and P. Grangier, J. Opt. Soc. Am. B **27**, A137 (2010).
[35] M. Mastriani, Sci. Rep. **13**, 21998 (2023).
[36] E. Shchukin and P. van Loock, Phys. Rev. Lett. **128**, 150502 (2022).
[37] M. B. Plenio, Phys. Rev. Lett. **95**, 090503 (2005).
[38] G. Vidal and R. F. Werner, Phys. Rev. A **65**, 032314 (2002).
[39] Q. Guo, S.-B. Zheng, J. Wang, C. Song, P. Zhang, K. Li, W. Liu, H. Deng, K. Huang, D. Zheng, X. Zhu, H. Wang, C.-Y. Lu, and J.-W. Pan, Phys. Rev. Lett. **121**, 130501 (2018).
[40] J. Majer, J. Chow, J. Gambetta, J. Koch, B. Johnson, J. Schreier, L. Frunzio, D. Schuster, A. A. Houck, A. Wallraff *et al.*, Nature (London) **449**, 443 (2007).